Chemo-hydrodynamic pulsations in simple batch A + B → C systems

Chemo-hydrodynamic pulsations in simple batch A+B→C systems

Marcello A. Budroni,[1, a)] Alessandro Polo,[1] Virat Upadhyay,[2] Adam Bigaj,[2] and Laurence Rongy[2]
[1)] *Department of Chemistry and Pharmacy, University of Sassari, Via Vienna 2, 07100 Sassari, Italy.*
[2)] *Nonlinear Physical Chemistry Unit, Service de Chimie Physique et Biologie Théorique, Université libre de Bruxelles, CP 231 - Campus Plaine, 1050 Brussels, Belgium.*

(Dated: February 24, 2021)

Spatio-temporal oscillations can be induced in batch conditions with ubiquitous bimolecular reactions, in the absence of any nonlinear chemical feedback, thanks to an active interplay between the chemical process and chemically-driven hydrodynamic flows. When two reactants A and B, initially separated in space, react upon diffusive contact, they can power convective flows by inducing a localized variation of surface tension and density at the mixing interface. These flows feedback with the reaction-diffusion dynamics, bearing *damped* or *sustained* spatio-temporal oscillations of the concentrations and flow field. By means of numerical simulations, we detail the mechanism underlying these chemohydrodynamic oscillations and classify the main dynamical scenarios in the relevant space drawn by parameters ΔM and ΔR, which rule the surface tension- and buoyancy-driven contributions to convection, respectively. The reactor height is found to play a critical role in the control of the dynamics. The analysis reveals the intimate nature of these oscillatory phenomena and the hierarchy among the different phenomena at play: oscillations are essentially hydrodynamic and the chemical process features t he localized trigger for Marangoni flows unstable towards oscillatory instabilities. The characteristic size of Marangoni convective rolls mainly determines the critical conditions and properties of the oscillations, which can be further tuned or suppressed by the buoyancy competition. We finally discuss the possible experimental implementation of such a class of chemo-hydrodynamic oscillator and its implications in fundamental and applied terms.

I. INTRODUCTION

Chemical reactions provide fundamental means not only for the synthesis of new products but also for the internal and spontaneous spatio-temporal self-organization of a system[1]. Oscillations and waves in inorganic chemical systems represent one of the most fascinating example of this chemically-driven order.

Inorganic chemical oscillations and waves find current application in different areas. One of the most prominent is the use of these systems as benchmark models for mimicking biological systems where waves play an efficient strategy for cooperative transport of information as it happens, for instance, in cellular slime molds[2] or giant honeybees[3]. Chemical oscillators are widely adopted in the imitation of cellular environments and understanding how biological functionalities can arise from the communication among oscillatory units[4–6]. In particular, ensembles of compartmentalized coupled chemical oscillators are exploited as "neurons" and related synchronization patterns used to develop unconventional computing in the way towards brain-like chemical machines, wetware and artificial intelligence[7,8].

A further challenge is represented by the use of complex oscillatory reactions in materials science, where they can inspire new design of smart materials[9]. To give a few examples, chemical oscillators can fuel chemomechanical behaviors in chemo-responsive materials, that can, in turn, provide substrates for locomotion[10] and be involved in promising strategies for drug delivery[11]. From the synthesis viewpoint, nano-patterned multilayer alloys can be obtained *via* periodic deposition driven by electrochemical oscillators[12].

In other cases, also pertinent to the realm of materials science, the onset of an oscillatory instability can be an unfavorable event, needing a fine control. This happens, for instance, in dissolution-driven self-propulsion, where periodic trajectory bumps can obstacle the efficiency and predictability of the self-propelled device[13]. Nonlinear and oscillatory behaviors may also affect the delivery of molecular hydrogen from the hydrolysis of borohydride salts, limiting the use of this process as a green alternative fuel in combination with PEM cells[14,15].

In order to control undesired nonlinear oscillations and design new viable approaches to autonomous chemical oscillations, it is indeed of paramount importance to master the broadest number possible mechanisms that can lead to oscillatory instabilities[16].

So far, studies on chemical oscillations have been at the heart of nonlinear chemistry. Over the last three decades, the innermost mechanisms for chemical oscillations in homogeneous closed systems have been elucidated[1,17,18], pointing to the need of far-from-equilibrium conditions and nonlinear chemical or thermal feedbacks interweaving the reaction intermediates. From a theoretical perspective these essential properties are exemplified by the first thermodynamically consistent model for chemical oscillators, the Brusselator model[19], and experimentally embodied in the prototype of batch chemical oscillators, the Belousov-Zhabotinsky (BZ) reaction[20], able to oscillate autonomously for hours. Systematic algorithms for designing "ad-hoc" chemical oscillators have been imple-

[a)] Electronic mail: mabudroni@uniss.it

mented in open flow reactors, where oscillatory dynamics can be obtained systematically thanks to a slow feedback reaction that periodically flips a bistable system between two steady states[21]. Nevertheless the whole landscape of chemicals and reactions that can effectively give rise to inorganic oscillators is restricted to a confined number of species and nonlinear processes[18].

Is it possible to design autonomous oscillations with more ordinary and general kinetics?

Recently, we have opened this perspective by showing how simple bimolecular reactions can yield spontaneous pulsatory behaviors, in the absence of any nonlinear or external chemical feedback[22]. Key for this behavior is an *active* interplay between the chemical process and chemically-driven hydrodynamics: by changing the local chemical composition and related properties (such as surface tension and density gradients), the reactive process activates *in-situ* the medium by triggering and sustaining convective flows. These, in turn, feedback with the spatio-temporal evolution of the chemical fields. Differently from *passive* chemohydrodynamics, where chemicals behave as scalars advected by externally imposed flows, this active loop provides an autonomous basis for complex dynamics[23].

Active chemohydrodynamics has been extensively explored in two main classes of systems.

One class relies on nonlinear kinetics, where chemically-driven hydrodynamics further complicates the spatio-temporal behaviors of already complex chemical structures such as fronts, waves and Turing patterns[24,25]. Self-propagating autocatalytic fronts can be periodically deformed by the antagonism between solutal and thermal density– or surface–driven flows in the presence of differential diffusion[26–28] or by the competition between buoyancy and Marangoni forces[29,30]. Front rippling occurs when the reaction triggers high surface tension gradients, as a consequence of mechanical stresses at the quasi-horizontal interface between the reacted and non-reacted fluid[31,32]. Progressive deformation and breakups of chemical waves and spirals due to surface-flows and gravitational currents were also found to drive these periodic patterns to segmented waves[33] and chemical turbulence[34].

A second research line, at the core of this work, focuses on the impact of simple localized chemical transformations on hydrodynamic instabilities. In this context, the classic A+B→C system[35], where two reactants A and B are initially separated in space and start to react upon diffusive contact, was widely adopted. The structural and dynamical properties of this reaction front (i.e. the zone where the production rate is non-zero) have been thoroughly analyzed[35,36] since it constitutes a paradigmatic model for understanding, among others, self-organized localized patterns like Liesegang bands and more complex microporous structures like chemical gardens, particularly promising in materials science and for understanding the formation of pre-biotic environments where life emerged[37,38].

The onset of chemically-driven convection in such A+B→C systems was found to severely modify the morphology of classic hydrodynamic patterns in vertically stratified systems[39,40] and to promote a wealth of spatio-temporal evolution of the chemical reaction due to buoyancy-, surface-tension-[41,42], or viscosity-driven[43] instabilities both in vertically[39,44] and horizontally oriented reactors[45].

Although the A+B→C systems have been studied at length in various problems ranging from chemistry to finance, evidence for pulsatory dynamics had never been reported. Periodic dynamics were induced by extending the problem to an A+B→ *Oscillator* case, where A and B are pool solutions containing separated reactants of a chemical oscillator[46–50], and the chance for oscillatory dynamics is embedded in the chemistry of the system.

Differently from previous approaches, in this work we exploit the active chemohydrodynamic interplay to power autonomous emergent pulsatory behaviors with the general class of A+B→C reactions. The localized reaction increases the surface tension across the mixing area, generating thereby a neat convergent stress at the liquid-air interface. The reaction can possibly decrease the local density, thus promoting an antagonistic upwardly oriented gravitational current in the reactive zone. In principle the reaction and related flows are not oscillatory, but their combination leads to the emergent oscillatory behaviors. A flavor of these dynamics is given in[22] and Fig.1, where the two main oscillatory scenarios are paralleled (see also supplementary material).

In the following we provide a detailed description of the model governing the dynamics of this system (section II). The resulting chemohydrodynamic oscillations both due to sole Marangoni flows and by antagonistic Marangoni and buoyancy forces are illustrated in sections III and IV. Here, thanks to an extended characterization of the oscillation properties, we single out favorable conditions and criteria for the emergence of these patterns and show how different regimes can be controlled by tuning the relative importance of the two competitive contributions to the flow. This analysis allows to understand more in-depth the nature of the phenomenon and suggests future implementation of chemohydrodynamic waves in experimental systems. These results are summarized in section V, before discussing fundamental and applied implications of this study in section VI.

II. MODEL

The system consists of a two-dimensional reactor of length L_X and height L_Z in a (X, Z) reference frame, where the Z axis is oriented vertically against the gravitational acceleration $\mathbf{g} = (0, -g)$. The reactor is supposed to be in isothermal conditions and open to the air on the top border, where the air-liquid interface is assumed to be non–deformable and evaporation is also neglected. The initial spatial distribution of the chemical species

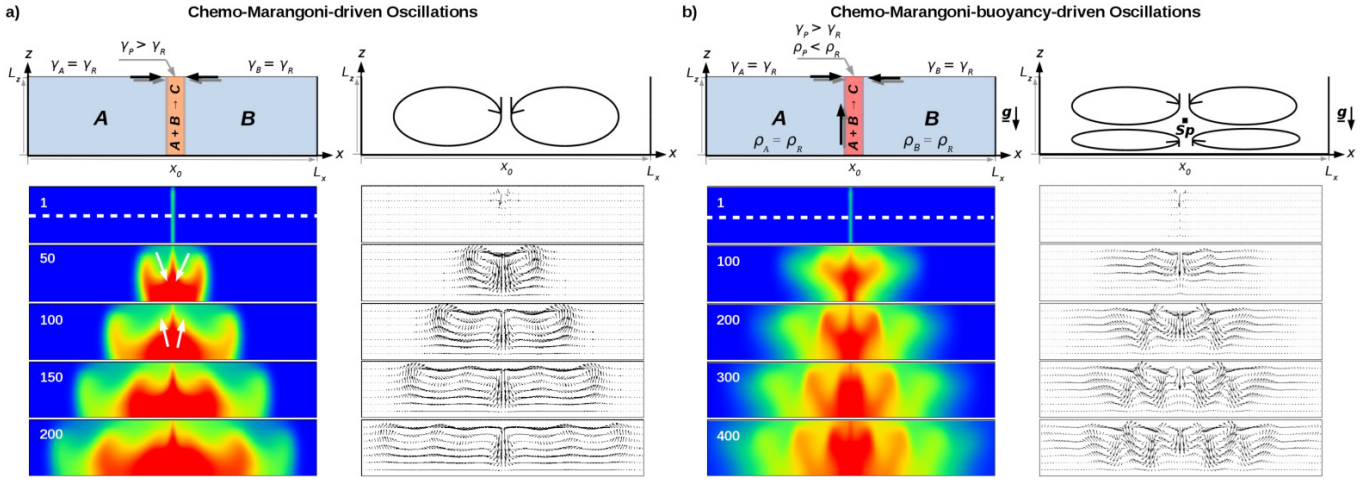

Figure 1. Typical (a) *Chemo-Marangoni damped oscillations* due to chemically-driven Marangoni flows and (b) *chemo-Marangoni-buoyancy sustained oscillations* arising when both buoyancy and surface tension forces are antagonistically at play in an A+B→C system. The initial configuration of the reactants and the related topology of the chemically-induced velocity field are sketched at the top of each panel. The two reactants A and B have the same surface tension $\gamma_A = \gamma_B = \gamma_R$ and density $\rho_A = \rho_B = \rho_R$, while in the reactive zone, where C forms, the surface tension locally increases $\gamma_P > \gamma_R$ and the density decreases $\rho_P \leq \rho_R$. The snapshots illustrate the spatio-temporal evolution of the chemical (c, on the left) and the velocity ($\mathbf{v}$, on the right) fields, respectively, during few oscillatory cycles. The arrows in panel (a) at times 50–100 indicate the flow-driven compression and RD relaxation of c. The black square in the velocity field cartooned at the top of panel (b) locates the stagnation point, Sp. These illustrative simulations were obtained by using the dimensionless parameters $\Delta M = 200$ and $\Delta R = 1.75$ discussed in the text.

concentrations A, B, C

$$(A, B, C) = (A_0, 0, 0) \text{ for } X < X_0 = L_X/2 \ \forall Z$$
$$(A, B, C) = (0, B_0, 0) \text{ for } X > X_0 \ \forall Z\,,$$
$$(A, B, C) = (A_0, B_0, 0) \text{ for } X = X_0 \ \forall Z\,,$$

describes the typical configuration of an A+B→C problem[35], cartooned at the top of Figs.1a and 1b. The pure reactant solutions A and B have surface tension γ_A and γ_B, and density ρ_A and ρ_B, respectively. The formation of the product C occurs upon diffusive mixing of the two reactants A and B across the initial contact line localized at X_0. In the reactive zone, the medium surface tension, γ, and the density, ρ, locally change, inducing convective transport (see top sketches in Figs.1a and 1b).

The resulting nonlinear dynamics is governed by a set of partial differential reaction-diffusion-convection (RDC) equations

$$\partial_t A + (\mathbf{V}\cdot\nabla)A = D_A\nabla^2 A - kAB\,, \quad (1)$$
$$\partial_t B + (\mathbf{V}\cdot\nabla)B = D_B\nabla^2 B - kAB\,, \quad (2)$$
$$\partial_t C + (\mathbf{V}\cdot\nabla)C = D_C\nabla^2 C + kAB\,, \quad (3)$$
$$\partial_t \mathbf{V} + (\mathbf{V}\cdot\nabla)\mathbf{V} = -\frac{1}{\rho_0}\nabla P + \frac{\mu}{\rho_0}\nabla^2\mathbf{V} - g\frac{(\rho-\rho_0)}{\rho_0}\,\mathbf{1}_z \quad (4)$$
$$\nabla\cdot\mathbf{V} = 0\,, \quad (5)$$

combined to the Marangoni boundary condition

$$\mu\partial_Z U = \partial_X\gamma \ \text{ at } \ Z = L_Z\,, \quad (6)$$

which includes shear stresses at the top free surface.

The evolution of the chemical fields $I = A, B, C$ described by eq. (1–3), is coupled to the incompressible Navier–Stokes equations (4–5) and the Marangoni condition (6) *via* the state equations for the density $\rho = \rho_0\left(1 + \frac{1}{\rho_0}\sum_I I\,\partial_I\rho\right)$ and surface tension $\gamma = \gamma_0\left(1 + \frac{1}{\gamma_0}\sum_I I\,\partial_I\gamma\right)$. In diluted solutions, ρ and γ can, indeed, be expressed as a linear combination of the chemical concentrations, modulated by the density solutal expansion coefficient and the surface activity of each I–th species, $\frac{1}{\rho_0}\partial_I\rho$ and $\frac{1}{\gamma_0}\partial_I\gamma$, respectively. ρ_0 and γ_0 are the solvent density and surface tension, respectively.

Hydrodynamic equations are written in the Boussinesq approximation, i.e. assuming that density changes only affect the gravitational force term $g\frac{(\rho-\rho_0)}{\rho_0}$ of eq.(4), where g is the gravitational acceleration and $\frac{(\rho-\rho_0)}{\rho_0}$ is the density variation due to the concentration changes with respect to the initial reference state of the solvent, ρ_0. $\mathbf{V} = (U, V)^T$ is the velocity field, μ is the dynamic viscosity, D_I are the diffusion coefficients of the chemical species, and P is the dynamic pressure.

The equation system can be casted in dimensionless form by using the reaction-diffusion (RD) scales for time, $t_0 = 1/(kA_0)$, length, $L_0 = \sqrt{D_A t_0}$ and concentration, A_0 (k is the kinetic rate constant of the reaction). From t_0 and L_0 the velocity and pressure scales are also derived as $V_0 = L_0/t_0 = \sqrt{D_A/t_0}$, $P_0 = \frac{\mu}{t_0}$, respectively. This leads to the following dimensionless equations:

$$\partial_t a + (\mathbf{v}\cdot\nabla)a = \nabla^2 a - ab \tag{7}$$
$$\partial_t b + (\mathbf{v}\cdot\nabla)b = \delta_b\nabla^2 b - ab \tag{8}$$
$$\partial_t c + (\mathbf{v}\cdot\nabla)c = \delta_c\nabla^2 c + ab \tag{9}$$
$$\partial_t \mathbf{v} + (\mathbf{v}\cdot\nabla)\mathbf{v} = S_c\left(-\nabla p + \nabla^2\mathbf{v} - \sum_{i=a,b,c} Ra_i(i)\,\mathbf{1}_z\right) \tag{10}$$
$$\nabla\cdot\mathbf{v} = 0\,, \tag{11}$$

where the variables are now all dimensionless. The Marangoni boundary condition now reads

$$\partial_z u = -\sum_i M_i\,\partial_x i_s\,, \tag{12}$$

where $i_s = a_s, b_s, c_s$ are the surface dimensionless concentrations of the chemical species at $z = L_z$.
The Schmidt number $S_c = \mu/D_A\rho_0$ gives the balance between momentum and mass diffusion. We set $S_c = 1000$, which is compatible with aqueous solutions where the water kinematic viscosity $\nu = \mu/\rho_0 = 0.0089$ cm^2 s^{-1} and typical values for the diffusivity of chemical species $D_I \in [10^{-6}, 10^{-5}]$ cm^2 s^{-1}. $\delta_i = D_I/D_A$ are the dimensionless relative diffusivities.

$$R_i = \frac{\partial_I\rho\, A_0 g L_0^3}{D_A\mu} \tag{13}$$

is the solutal Rayleigh number of the I–th species, tuning the specific contribution of each species to the local density, while the solutal Marangoni number

$$M_i = -\frac{1}{\mu}\sqrt{\frac{A_0}{kD_A}}\,\partial_I\gamma\,, \tag{14}$$

quantifies the specific contribution of the I–th species to the local surface tension.
In this dimensionless description, the letters have the same meaning as in dimensional form where capital letters have been used except for time, density and surface tension. The dimensionless density is $\tilde{\rho} = \frac{\rho-\rho_0}{\rho'} = \sum_i R_i\, i$ (with $\rho' = \frac{\mu}{t_0 L_0 g}$ defining the density scale) and the dimensionless surface tension $\tilde{\gamma} = \frac{\gamma-\gamma_0}{\gamma'} = -\sum_i M_i\, i_s$ (where $\gamma' = \frac{\mu L_0}{t_0}$ is the surface tension scale).
By taking the curl of both sides of eq.(10), the pressure term ∇p can be eliminated, and using the relations that link the dimensionless velocity field $\mathbf{v} = (u, v)$ to the vorticity $\omega = \nabla\times\mathbf{v}$ and to the stream function, ψ, $u = \partial_z\psi$ and $v = -\partial_x\psi$[29], we obtain the RDC equations in the ω–ψ form

$$\partial_t a + (\partial_z\psi)\,\partial_x a - (\partial_x\psi)\,\partial_z a = \nabla^2 a - ab\,, \tag{15}$$
$$\partial_t b + (\partial_z\psi)\,\partial_x b - (\partial_x\psi)\,\partial_z b = \delta_b\nabla^2 b - ab\,, \tag{16}$$
$$\partial_t c + (\partial_z\psi)\,\partial_x c - (\partial_x\psi)\,\partial_z c = \delta_c\nabla^2 c + ab\,, \tag{17}$$
$$\partial_t\omega + (\partial_z\psi)\,\partial_x\omega - (\partial_x\psi)\,\partial_z\omega = S_c\left(\nabla^2\omega - \sum_{i=a,b,c} R_i\,\partial_x i\right) \tag{18}$$
$$\nabla^2\psi = -\omega\,, \tag{19}$$

coupled to the Marangoni boundary condition $\omega = \sum_i M_i\,\partial_x i_s$, with $i = a, b, c$.
To keep the system as simple as possible and ensure a symmetrical development of the reactive zone[35,36,41,44], we assume that initial reactant solutions present the same properties: equal initial concentration, $A_0 = B_0$, surface tension, $\gamma_A = \gamma_B = \gamma_R$, density, $\rho_A = \rho_B = \rho_R$ and diffusivity, $\delta_b = 1$. As a result, the chemical front propagates into a "uniform" medium and initial changes of surface tension and density ($\gamma_P > \gamma_R$, $\rho_P < \rho_R$) can only be ascribed to the reaction-diffusion process and not to unbalanced properties of the reactants, such as differential diffusion. Moreover, taking into account the conservation of the chemical concentrations valid if also $\delta_c = 1$, $a + b + 2c = 1\,\forall\, x, z, t$, we can directly reconstruct the dimensionless concentration field of the product, c from a and b. The final form of the system writes

$$\partial_t a + (\partial_z\psi)\,\partial_x a - (\partial_x\psi)\,\partial_z a = \nabla^2 a - ab\,, \tag{20}$$
$$\partial_t b + (\partial_z\psi)\,\partial_x b - (\partial_x\psi)\,\partial_z b = \nabla^2 b - ab\,, \tag{21}$$
$$\partial_t\omega + (\partial_z\psi)\,\partial_x\omega - (\partial_x\psi)\,\partial_z\omega = S_c\left(\nabla^2\omega - \Delta R\,(\partial_x a + \partial_x b)\right) \tag{22}$$
$$\nabla^2\psi = -\omega\,, \tag{23}$$

with the Marangoni boundary condition $\omega = \Delta M\,(\partial_x a_s + \partial_x b_s)$.
Here $\Delta R = R - R_c/2$ and $\Delta M = M - M_c/2$, with $R = R_a = R_b$ and $M = M_a = M_b$ because we consider that the reactants have the same contribution to the density and the surface tension. The solution density and surface tension read $\tilde{\rho} = \Delta R(a + b) + R_c/2$ and $\tilde{\gamma} = -\Delta M(a_s + b_s) - M_c/2$, respectively.
Within this parametric formulation, the number of parameters tuning the relative importance of solutal buoyancy and surface tension contributions to convective flows, reduces from six (the Rayleigh and the Marangoni numbers of the 3 species in the system) to ΔR and ΔM. Positive ΔR and ΔM mean that the density decreases while the surface tension increases during the reaction.
The problem defined by eqs. (20–23) is closed by no-flux boundary conditions for the chemical concentrations at the four boundaries of the reactor, no-slip conditions for the velocity field at the three solid boundaries and, as mentioned above, Marangoni boundary conditions at the air-liquid interface at $z = L_z$.
To compare the system dynamics in closed and open conditions, additional simulations are carried out by considering fixed boundary values for the chemical

species:

$$(A, B, C) = (A_0, 0, 0) \text{ at } X = 0 \ \forall Z, t$$
$$(A, B, C) = (0, B_0, 0) \text{ at } X = L_x \ \forall Z, t\,.$$

This mimics a constant lateral feeding and exhaustion of the initial reactants and of the product. RDC equations (20–23) are solved numerically by using the Alternating Direction Implicit Method (ADI) proposed by Peaceman and Rachford[51]. We consider a spatial domain of dimensionless length $L_x \in [125, 256]$ and variable height L_z, discretized over a grid with meshing $h_x = h_z = 0.25$. Simulations are run using the integration time step $h_t = 1 \times 10^{-5}$.

III. CHEMO-MARANGONI OSCILLATIONS

A. Phenomenology

Chemo-Marangoni oscillations occur when surface stresses due to chemically-induced Marangoni flows are dominant (either for negligible gravitational effects, i.e. $\Delta R \to 0$, or in very shallow layers, i.e. small values of L_z). When ΔM is beyond a critical threshold ΔM_{crit} (the actual value slightly depends on L_z), spatio-temporal oscillations of the chemical and the velocity fields can nucleate at x_0 and develop symmetrically towards the lateral borders (see Fig. 1a and supplementary material).

The mechanism of wave formation follows a local increase of the surface tension γ across the area where the reaction consumes A and B to form C. This bears convergent Marangoni flows at the air-liquid surface and, by continuity a vertical down-flow at x_0 that advects the product towards the rigid bottom boundary. This causes the deformation of C concentration field into two symmetrical fronts (see arrows in snapshots at $t = 50$). The return flow amplifies the extent of these fronts, advects the fluid from one side to the other, sweeping c towards the top of the reactor. The consequent formation of two new spots where surface tension increases, modifies the velocity field, favoring the splitting of the two initial convective rolls and weakening the vertical convective forcing around x_0. The front of c can thus relax from the reactor bottom upwards (see arrows in the snapshot at $t = 100$). After the lateral dissipation of the symmetric waves the vertical down-flow at x_0 that opposes to this RD relaxation reinforces again and restores initial conditions for a novel oscillatory cycle. The diffusively-driven transverse feedback mechanism that recreates the sharp surface concentration gradient feeding the downward Marangoni forcing, progressively weakens because of the reactant consumption and species diffusion and, as a consequence, waves damp out. Note that during the whole dynamics the reaction zone (where the reaction rate $ab \neq 0$) remains essentially localized across x_0.

The whole spatio-temporal deployment of these Marangoni-driven *damped oscillations* is illustrated in the space-time plot of Fig.2a, where a horizontal concentration profile of c taken at $L_z/2$ (see dashed line in the first snapshot of Fig.1a) is reported as a function of time. The correspondent oscillatory hydrodynamic field is shown in Fig.2b, where we map the evolution of the stream function ψ. ψ minima (in blue) and maxima (in red) describe clockwise and counter-clockwise convective rolls, respectively.

The topology of these space-time maps represents a sort of fingerprint of the chemohydrodynamic waves, qualitatively preserved when changing the values of the control parameters. Dynamical information are embedded in the inherent timeseries obtained by plotting c and ψ at a fixed representative point of the reactor, as indicated by the white dashed lines in the space-time plot of Fig.2a. The local timeseries show transient *damped* oscillations. The damped character is preserved even by keeping the system far-from-equilibrium with a lateral influx of the initial reactants (compare circles (batch) and the solid line).

Local timeseries and space-time plots are used to extract the characteristic oscillation period, T, and the spatial characteristic length of the waves, λ. The oscillation period is obtained as the interval elapsed between the two first successive peaks of the oscillatory timeseries which are the most representative of far-from-equilibrium conditions in our batch system. The position of ψ extrema and their relative distance were used, as cartooned in Fig. 2b to define the spatial characteristic wavelength, λ of the waves. The dependencies of T and λ are then characterized in terms of the main control parameters ΔM, ΔR and L_z. T and λ are also used to compute the dispersion relation, relating the waves phase speed $v_p = \lambda/T$ as a function of their characteristic wavelength. Concretely, an estimate of v_p is given by the slope of the waves deployment in the spatio-temporal plots in the range showing a stable constant drifting, namely after nucleation and before the interaction with the lateral borders.

B. Controlling chemo-Marangoni oscillations

1. Role of ΔM

As shown in our previous work[22], there is a critical threshold $\Delta M > \Delta M_{crit}$ beyond which chemo-Marangoni pulsations can occur. This condition implies that the surface tension must increase sufficiently in the reaction zone. In parametric terms, this is easily satisfied when the Marangoni number of the product, M_c, is much smaller than that characterizing the initial reactants, M. If we express M_c in terms of M, $M_c = \zeta M$, we can see that the condition $\Delta M > \Delta M_{crit}$ can also be met for values of M_c comparable or even larger than M,

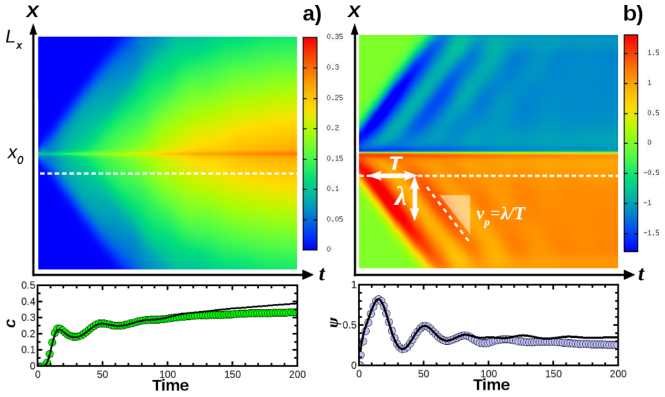

Figure 2. Top panels: Space-time plots ($L_x = 128 \times t = 200$) describing a) the chemical (c) and b) the hydrodynamic (ψ) evolution of a typical chemo-Marangoni scenario in open conditions ($\Delta M = 250, L_z = 12$). The plots are built at $z = L_z/2$ (for illustration see the white line traced in the first snapshot of Fig.1a). Species c ranges between 0 (blue areas) and 0.5 (red areas), while ψ varies between -2 (blue areas) and 2 (red areas). T, λ and v_p indicate the characteristic oscillation period, spatial length and phase speed, respectively. Bottom panels: the local timeseries of c and ψ at a representative point of the reactor ($x_0 - 10, L_z/2$) indicated by the dashed line in the spacetime plots. The circles correspond to the the batch system while the solid lines describe the system maintained in open conditions by the lateral feeding of the reactants.

provided that

$$M > \frac{2}{2-\zeta}\Delta M_{crit} \ , \tag{24}$$

with $\zeta \in [0, 2)$. This means that when M is large enough such that eq.(24) holds (reactants with very low surface tension), the occurrence of oscillations is essentially independent on the specific contribution of the product. A local increment of the surface tension emerges autonomously from the reactive process that consumes the species responsible for low surface tension. This condition enlarges the number of chemo-physical systems that can undergo this instability.

Although the occurrence of this instability is very sensitive to ΔM, both T and λ do not vary significantly with this parameter (see Fig.3a showing the period and the wavelength dependence on L_z for different ΔM).

2. Role of L_z

Chemo-Marangoni spatio-temporal oscillations present a strong dependence on L_z. The length of convective rolls follows a linear relation with L_z ($\lambda \sim L_z$) that, in turn, controls T (Fig.3a). In particular, the period at which waves are emitted from the centre grows by increasing L_z, scaling as $T \sim L_z^2$. Wave formation is suppressed below a critical height L_c (this threshold slightly shifts

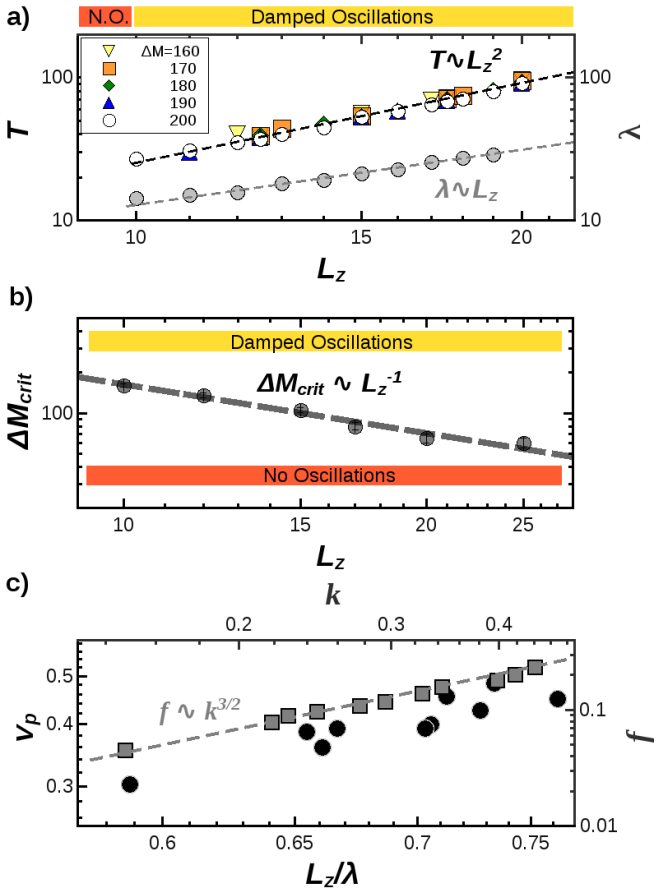

Figure 3. Characterization of *damped oscillations* in the chemo-Marangoni scenario. a) Dependence of the oscillation period, T (left axis), and the characteristic length, λ (right axis), on L_z for different ΔM (adapted with permission from Phys. Rev. Lett. 122, 244542 (2019). Copyright 2019 American Physical Society). The bar at the top of the plot indicates the dynamical regimes of the system throughout L_z-domain: the red bar refers to a non-oscillatory (N.O.) scenario corresponding to symmetric fronts; the yellow bar indicates *damped* oscillations. b) Dependence of the critical ΔM upon L_z. c) Black circles: dependence of the phase speed of chemo-Marangoni waves, v_p (left axis), on the relative wavelength L_z/λ (bottom axis) ($\Delta M = 200$); gray squares: dispersion relation tying the angular frequency, $f = 2\pi/T$ (right axis) to the wavevector $k = 2\pi/\lambda$ (top axis).

to higher values when ΔM decreases). Different dynamical regimes occurring in the L_z-domain are summarized at the top of Fig.3a. Here the red bar refers to a non-oscillatory (N.O.) scenario corresponding to symmetric fronts departing from x_0 towards the lateral borders; the yellow bar indicates *damped* oscillations.

The layer thickness L_z represents a determinant parameter that can modulate the balance between the reaction-diffusion and the convective timescales. The relation describing this critical interplay is captured by Fig.3b, where the threshold ΔM_{crit} (above which oscillations are observed in numerical experiments) is plotted as a func-

tion of L_z. The trend separating the oscillatory from the non-oscillatory domain shows that ΔM_{crit} is inversely proportional to L_z, with an exponent close to 1 (1.11 $\pm$ 0.08). A justification of this dependence can be derived through phenomenological arguments[22]. Chemo-Marangoni waves result from the transverse competition between the horizontal Marangoni-driven return flow and the vertical RD relaxation that tends to level out the local concentration gradients at the top surface. For oscillations to start, the Marangoni timescale τ_{Ma} compatible with the wave characteristic length λ has to be smaller than the reaction-diffusion timescale τ_{RD} needed to cover a distance $\mathcal{O}(L_z)$, $\tau_{RD} \sim L_z^2$. τ_{Ma} can be obtained as the ratio between the spatial characteristic length of the convective roll, λ, and the associated horizontal velocity of a parabolic Marangoni return flow responsible of the shape and the entity of the chemical front deformation. The typical profile of the horizontal component of the Marangoni return flow follows the form $u_{Ma} \sim \pm\frac{L_z}{2}\Delta M\,(\frac{3}{2}\hat{z}-1)\hat{z}$ (where $\hat{z}=z/L_z$, and positive and negative solutions apply to $x<x_0$ and $x>x_0$, respectively), with a maximum at $z=\frac{1}{3}L_z$ related to the bulk flow, and a sign inversion at $z=\frac{2}{3}L_z$ above which the linear shear flow prevails[31,52]. In Fig.4 we show that this form (traced with symbols) fits well the velocity profiles developing in our system (solid curves), particularly across the tip of the chemical front where the surface concentration gradients, $\mathrm{Grad}_s(x)=\partial_x a_s+\partial_x b_s$, decrease monotonically and converge to a common behavior for different values of ΔM.

The absolute value of the maximum of the parabolic profile $|u_{Ma}|$ at $z=\frac{1}{3}L_z$ can thus be used to define the scaling of the characteristic Marangoni velocity which, assuming $2L_z-1\approx 2L_z$, reads $|u_{Ma}|\sim(\Delta M)^{-1}$. Since $\lambda\sim Lz$ (Fig. 2a), this gives $\tau_{Ma}\sim\lambda/|u_{Ma}|\sim(\Delta M)^{-1}$. By imposing $\tau_{Ma}<\tau_{RD}$, we obtain that $L_z>L_c\sim(\Delta M)^{-1}$ or, equivalently, $\Delta M_{crit}\sim L_z^{-1}$, which is in good agreement with the numerical analysis of Fig.3b.

We finally characterize the speed of the chemo-Marangoni waves. For classic RD chemical waves developing in homogeneous excitable or oscillatory media[53–55], the speed of the waves is strictly related to the characteristic wavelength (or period). The *normal* profile of this dispersion relation follows a monotonic and decelerated growth from a minimal velocity value (associated to the minimal wavelength for a stable wave train) to the asymptotic velocity of a solitary pulsation. In other words, short wavelength wave-train develop slower. For chemohydrodynamic waves, we found a direct dependence not only on λ but also on the layer depth, L_z. In Fig.3c we combine these two dependencies by plotting the wave speed v_p versus the relative wavelength, L_z/λ. The graph shows that waves characterized by longer relative wavelengths (short λ compared to L_z) propagate faster (the opposite as compared to chemical RD waves). This is confirmed for different values of ΔM and considering several depths of the reactor. A dispersion relation $f^2\sim k^3$ (where $f=2\pi/T$ and $k=2\pi/\lambda$) consistent with

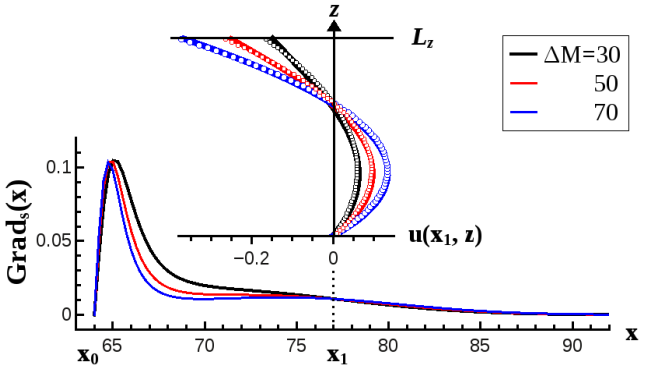

Figure 4. Vertical profiles of the horizontal velocity of the Marangoni return-flow, u, at $x_1=77$ and $t=30$ for different values of ΔM ($L_x=128$ and $L_z=17$). Solid curves describe the profiles extracted from numerical simulations while overlapping symbols show the related fitting *via* the form $u_{Ma}=-\frac{L_z}{2}\Delta M\,(\frac{3}{2}\hat{z}-1)\hat{z}\times\mathbf{cost}$, where $\hat{z}=z/L_z$ and **cost** is a space-dependent fitting constant related to the surface concentration gradient $\mathrm{Grad}_s(x)=\partial_x a_s+\partial_x b_s$. The profiles $\mathrm{Grad}_s(x)$ for the same values of ΔM are also shown for the spatial domain $x\geq x_0$.

that of typical capillary hydrodynamic waves[56] is also recovered and shown with gray squares in Fig.3c (refer to top-right axes). This allows us to conclude that the observed chemo-Marangoni oscillations adhere to the main characteristics of hydrodynamical waves.

IV. CHEMO-MARANGONI-BUOYANCY OSCILLATIONS

A. Phenomenology

Chemo-Marangoni-buoyancy oscillations occur when an antagonistic interplay of chemically-driven gravitational currents and Marangoni flows is at play. Here, the formation of C, by decreasing the local density of the medium, generates a vertical up-flow opposing and partially counterbalancing the Marangoni-induced convergent flow. As compared to chemo-Marangoni scenario, the topology of the velocity field becomes more complex, with the formation of two new upwardly oriented convective rolls at the bottom of the reactor that reduce the extent of the Marangoni-related rolls at the top (see sketches in the top panels of Fig.1b).

An illustration of three typical oscillatory cycles in this system is given in Fig.1b (and in the supplementary material) with the evolution of the chemical field, c, paralleled to the corresponding velocity field, $\mathbf{v}$. An extended representation of the dynamics is described in the space-time plots of Fig.5 (built using concentration and ψ profiles at $L_z/2$ as indicated by the dashed line in the first snapshot of Fig.1b).

Conceptually, the mechanism follows similar steps as in

the pure Marangoni scenario: surface-tension-triggered convergent down-flow starts upon formation of the product which is then pushed towards the bottom. However buoyancy forces combine here to RD processes to bounce back the local accumulation of the less dense product towards the reactor surface. Gravitational currents therefore amplify and sustain the oscillatory mechanism as can be seen in the local timeseries describing the dynamics at a representative point. The ψ timeseries reported in Fig.5b (bottom) shows an initial growth of the oscillation, followed by a smooth decay of the oscillation amplitude as the system evolves towards the equilibrium. Oscillations dampen over a longer time interval as the reactor width L_x increases. The enhancing action of buoyancy flows is also found by simulating the analogue open-system, with a lateral convection-less feeding of fresh reactants. Here we can stabilize the oscillation amplitude for a longer time by maintaining the system in far-from-equilibrium conditions. This picture is different from the pure chemo-Marangoni-driven instability where oscillations dampen out shortly and monotonically even in open conditions. We refer to this scenario as *sustained oscillations*.

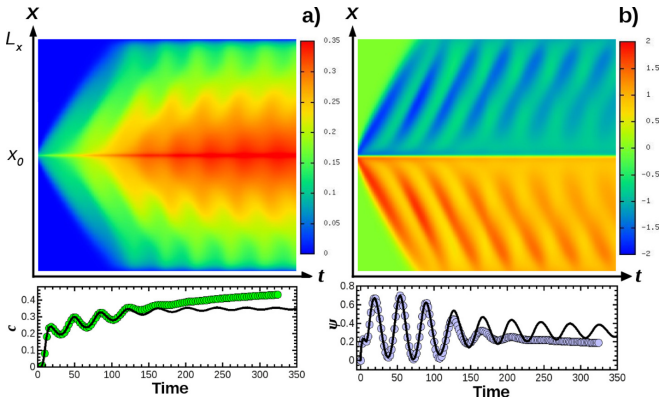

Figure 5. Space-time plots ($L_x = 128 \times t = 300$) describing (a) the chemical and (b) the hydrodynamic evolution of typical *sustained oscillations* promoted by a chemo-Marangoni-buoyancy interplay ($\Delta M = 250, \Delta R = 1.5, L_z = 12$). The plots are built at $L_z/2$, along the white line traced in the first snapshots of Fig.1b. Species c in (a) ranges between 0 (blue areas) and 0.5 (red areas), while ψ in (b) varies between -2 (blue areas) and 2 (red areas). Each panel shows at the bottom the local timeseries obtained by extracting c and ψ at a representative point of the reactor ($x_0 - 10, L_z/2$). The circles correspond to the the batch system while the solid lines describe the system maintained in open conditions by the lateral feeding of the reactants.

B. Controlling chemo-Marangoni-buoyancy oscillations

The birth and maintenance of chemo-Marangoni-buoyancy oscillations result from a delicate balance between Marangoni- and buoyancy-driven forces that alternately dominate the dynamics. Once the oscillatory instability is triggered *via* surface-tension-driven flows (i.e. $\Delta M > \Delta M_{crit}$), tuning the interplay between opposite Marangoni- and buoyancy-driven forces allows to enhance the oscillatory mechanism, modify the characteristics of the oscillatory regimes or even quench oscillations.

At fixed ΔM, ΔR and L_z control the importance of gravitational currents. Increasing ΔR or L_z increases buoyancy forcing and, as a result, the vertical extent of the Marangoni-dominated convection is reduced by larger buoyancy competitive convective rolls at the reactor bottom. The relative weight of the two contributions to the flow can be dynamically followed through the location of the stagnation point Sp, where the vertical velocity along the z-axis at x_0 changes sign (see sketch at the top of Fig.1b). In particular, when buoyancy-driven forces are dominant (high values of ΔR or L_z), Sp is closer to the surface since the less dense product is pushed upwards; *viceversa* Sp approaches the reactor bottom if gravitational currents are secondary as compared to Marangoni effects.

1. Role of ΔR

$\Delta R > 0$ switches on competitive buoyancy forces. Increasing ΔR (with ΔM fixed) strengthens the upwards response to Marangoni flow, driving a progressive transition from *damped* to *sustained* oscillations and back to non-oscillatory regimes. In the oscillatory domain ΔR modulates the oscillation period. A parametric classification of the main dynamical scenarios is given in the space $(\Delta M, \Delta R)$ in Fig.6. Suitable conditions for sustained oscillations span roughly the region $\Delta M \in [130, 250]$ and $\Delta R \in (0, 3.5]$, $L_z = 20$. More extreme values of ΔM may also be compatible with the oscillatory instabilities but we didn't explore that region. A transition from pure chemo-Marangoni *damped* (yellow diamonds) to *sustained* (green circles) oscillations sharply occurs as soon as $\Delta R > 0.5$ and $\Delta M > \Delta M_{crit}$: indeed relatively small buoyancy contribution to the flow can enhance oscillations independently of ΔM. On the contrary, the reverse route to non-oscillatory regimes at larger ΔR (*sustained* $\rightarrow$ *damped* $\rightarrow$ no-oscillations) is much more modulated by ΔM.

The influence of ΔR on the system dynamics is further illustrated in Fig.7a, where we report representative oscillatory timeseries for different values of ΔR ($\Delta M = 200$, $L_z = 20$). Buoyancy contribution sustains the oscillatory mechanism in a circumscribed range of ΔR (1.25 and 2), while larger values cause oscillations to dampen.

A favourable antagonism for the emergence of spatio-temporal oscillations thus requires surface-tension forces to overcome buoyancy ones. This picture can be conveniently described in terms of Sp. Accordingly, the spatio-temporal evolution of Sp in the oscillatory regimes show that the spatial extent of the Marangoni-related domain

(given by $L_z - Sp$) grows in time, first monotonically, and then following a periodic evolution when the system starts to pulsate (Fig.7b). Oscillations can start if $L_z - Sp > L_c$ (indicated by the black dashed line), i.e. beyond the same critical height threshold L_c where the oscillatory instability starts in the pure chemo-Marangoni scenario. Conversely, if buoyancy contribution prevails over Marangoni flows, the extent of buoyancy–driven convective rolls progressively grows upwards and the vertical residual space to initiate the oscillatory mechanism *via* surface tension effects falls below L_c, when oscillations cannot start or be maintained.
$L_z - Sp > L_c$ thus identifies a phenomenological criterion for oscillations to occur.
Fig. 8a describes how ΔR modulates the oscillation period through the different oscillatory regimes, indicated in the top axis. Changes in ΔM, also included in Fig.7a, show a negligible impact on the oscillation period. By contrast, in analogy with the trend observed by decreasing L_z in the chemo-Marangoni scenario (compare with Fig.3a), the shrinking of the characteristic size of Marangoni convective rolls due to increasing ΔR goes in parallel with a decline of the characteristic oscillation period ($T \sim \Delta R^{-1}$). This analysis suggests that surface-tension-driven convection is the trigger for the onset of chemohydrodynamic oscillations (both *damped* and *sustained* ones), imposing critical conditions for their possible occurrence, but it also mainly determines the characteristic space length of the phenomenon.
The dependence of phase velocity of chemo-Marangoni-buoyancy waves, v_p, on the intensity of the gravitational currents, as controlled by ΔR, is analyzed in Fig. 8b. $v_p(\Delta R)$ considered at the reactor top and half converge to a similar increasing trend suggesting that the buoyancy contribution enhances the propagation of these waves. By contrast, the dynamics at the reactor bottom is negligibly affected by this parameter.

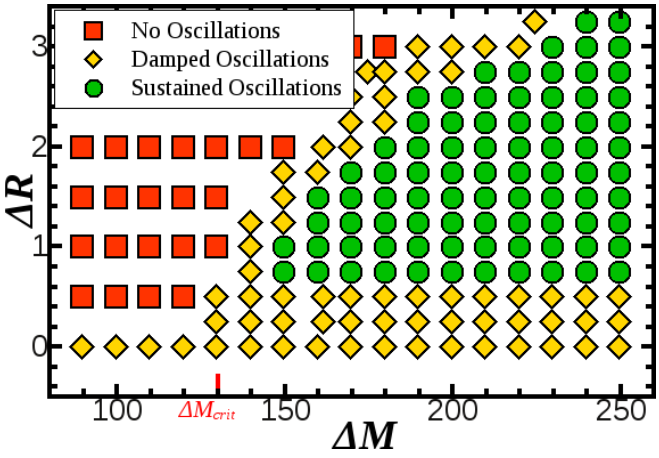

Figure 6. Overview of possible chemohydrodynamic scenarios due to an antagonistic interplay between chemically-driven Marangoni and buoyancy convection in the parametric space (ΔM, ΔR) with $L_z = 20$. ΔM_{crit} represents the critical ΔM threshold for waves in the chemo-Marangoni-buoyancy regime.

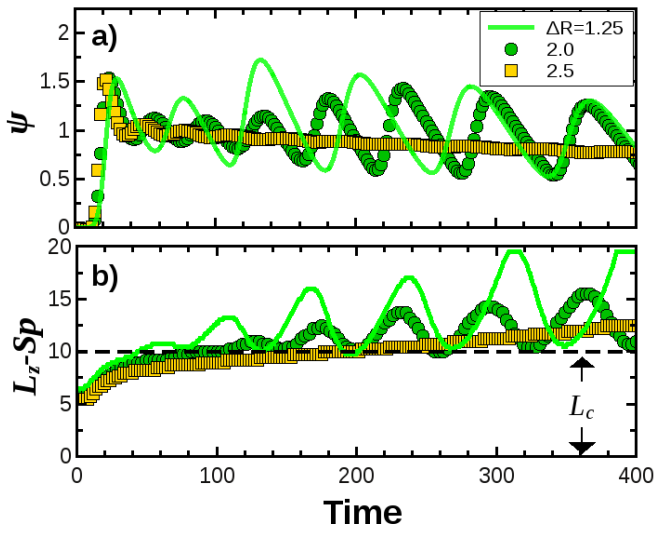

Figure 7. Effect of ΔR on the chemo-Marangoni-buoyancy oscillations. a) Local timeseries of ψ at a representative point of the reactor ($x_0 - 20$, $L_z/2$) for 3 different values of ΔR ($\Delta M = 200$, $L_z = 20$) and b) corresponding evolution of the stagnation point Sp.

2. Role of L_z

The possible scenarios obtained by varying buoyancy forces *via* L_z are shown in Fig.9, where we report a) ψ local timeseries and b) the dynamics of the corresponding stagnation point normalized over L_z, $(L_z - Sp)/L_z$, for different reactor heights (at fixed ΔM and ΔR).
In the oscillatory regimes where buoyancy effects are weak (typically for $L_z \to L_c$), we recover the characteristic *damped* dynamics of pure chemo-Marangoni-driven instability (yellow dot-dashed lines). Here the Marangoni domain, $(L_z - Sp)$, grows monotonically and stabilizes towards L_z.
Progressively increasing L_z, buoyancy forces, though weaker than surface tension-driven flows, increase and actively contribute to the upward-oriented relaxation of the chemical front. As a consequence, $(L_z - Sp)/L_z$ initially grows in time but in a "decelerated" way and, beyond the critical value L_c/L_z, can undergo a periodic evolution consistent with *sustained oscillations*.
The maximal reactor height for which chemo-Marangoni-buoyancy oscillations can occur is expected to be bounded by the capillary length, $L_{cap} = \sqrt{\frac{\gamma}{\rho g}}$, which gives the equilibrium between gravitational and surface forces and, in our dimensionless model, scales as $L_{cap}/L_0 \sim \sqrt{\frac{\Delta M}{\Delta R}}$. For $L_z > L_{cap}/L_0$ buoyancy forces will prevail.
The analysis of the stagnation point dynamics allows

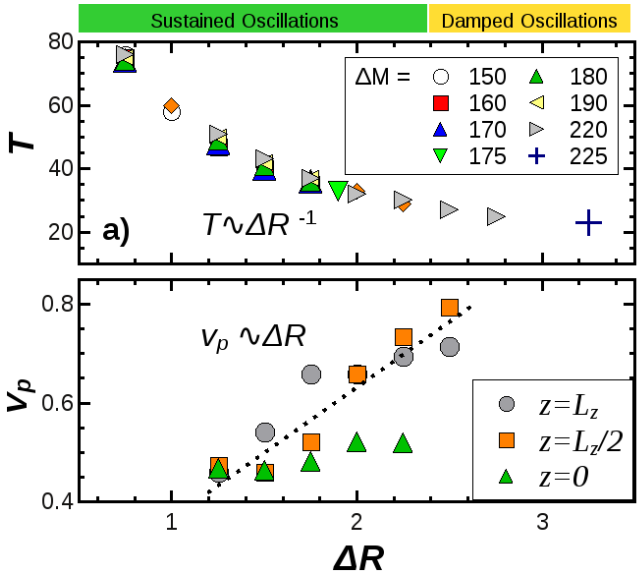

Figure 8. Characterization of chemo-Marangoni-buoyancy spatio-temporal oscillations as a function of ΔR. a) Dependence of the oscillation period, T, on ΔR for different ΔM (adapted with permission from Phys. Rev. Lett. 122, 244542 (2019). Copyright 2019 American Physical Society). The bar at the top of the plot indicates the dynamical regimes of the system in the ΔR domain. The yellow and green boxes refer to *damped* and *sustained* oscillatory dynamics, respectively. b) Dependence of the phase speed, v_p, of chemo-Marangoni waves (considered at different reactor depths) on ΔR ($\Delta M = 200$, $L_z = 20$). The dashed line is to guide the eye.

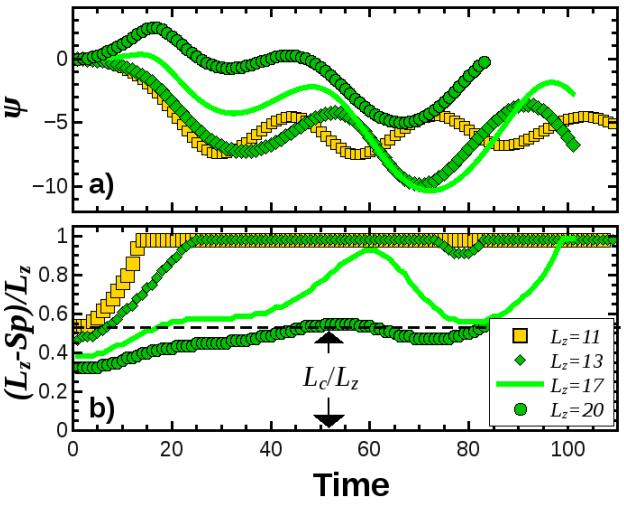

Figure 9. Influence of L_z on chemo-Marangoni-buoyancy oscillations. a) Local timeseries of ψ at a representative point of the reactor $(x_0 - 20, L_z/2)$ for 4 different values of L_z and b) corresponding evolution of the normalized complementary stagnation point $(L_z - Sp)/L_z$ ($\Delta M = 225$, $\Delta R = 1.75$). The yellow dashed-dotted line describes a *damped* oscillatory scenario, while green dashed, dotted and solid lines identify *sustained* oscillatory scenarios.

not only to isolate critical conditions for this oscillatory scenario, but also to understand the characteristic non-trivial dependence of the initial oscillation period upon L_z. This traces a tent-shaped profile with a maximum at L_{max} (see Fig.10a and 11a).

In the first branch, as L_z increases, the oscillation period increases. Here Marangoni convection governs the dynamics and an increment in the reactor height enlarges the size of the related convective rolls. These approach the whole reactor height available and thus $(L_z - Sp)/L_z \to 1$. The oscillation period, imposed by the characteristic length of the Marangoni convective rolls, increases accordingly.

The trend changes when L_z is further augmented beyond L_{max}. Here buoyancy-driven flows compensate the Marangoni-related forcing, decreasing the spatial characteristic length of chemohydrodynamic waves and, in turn, the oscillation period. The maximum of $T(L_z)$ thus indicates the switch point where buoyancy-driven flows, dynamically built during the induction period before the first oscillatory cycle, oppose effectively Marangoni forcing, such that the stagnation point cannot approach the reactor bottom, where $(Lz - Sp)/L_z = 1$.

The shape and the linear scaling of the ascending branch of $T(L_z)$ profiles (Fig.11a) are preserved for different values of ΔM and ΔR (slope $0.45(\pm 0.02)$). However, when ΔR is increased, L_{max} is shifted to lower values since these ΔR and L_z have an analogous effect on the strength of the buoyancy contribution and, hence, the value of L_z needed to counterbalance Marangoni forces decreases if ΔR increases. Fig.11b shows that the conservation relation between these two parameters obeys $L_{max}\Delta R^{1/3} = \text{const}$, which is compatible with eq. (13), linking the Rayleigh numbers to the spatial scale.

We finally analyze the properties of the phase speed for these chemohydrodynamic waves that, as mentioned above, is strictly dependent on the reactor depth, as accounted by the relative wavelength L_z/λ. In Fig.9b we can observe how the scaling of v_p abruptly changes when $L_z/\lambda \sim 0.5$. Consistently with the information embedded in the period profile $T(L_z)$, this minimum marks the transition from the Marangoni- (left branch) to buoyancy-controlled (right branch) dynamics. Data extracted at the top and half of the reactor height lie on a similar trend while the wave dynamics at the bottom shows a different pattern and no significant dependence on L_z. This is a further indication that the spatio-temporal behavior of chemo-Marangoni-buoyancy waves mainly takes place in the reactor top-half.

V. DISCUSSION

Spatio-temporal chemical oscillations can develop in simple A+B→C reactions. This process works in batch

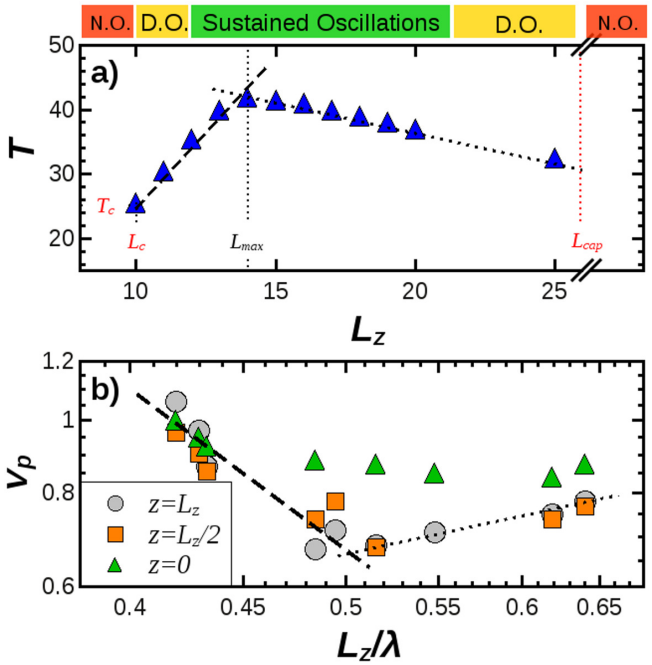

Figure 10. Characterization of chemo-Marangoni-buoyancy spatio-temporal oscillations. a) Tent-shaped profile of the oscillation period, T as a function of the reactor height L_z ($\Delta M = 200$, $\Delta R = 1.75$). L_c and T_c identify the lower critical reactor height for oscillations and related period, L_{max} and L_{cap}/L_0 locate the maximum of $T(L_z)$ and the capillary length (this is only included for the sake of illustration), respectively. The bar at the top of the plot describes different dynamical regimes over the L_z domain: the red, yellow and green boxes refer to non-oscillatory (N.O.), *damped* (D.O.) and *sustained* oscillatory dynamics. b) Dependence of the wave speed (v_p) of chemo-Marangoni-buoyancy waves (considered at different depths of the reactor) on the relative wavelength L_z/λ.

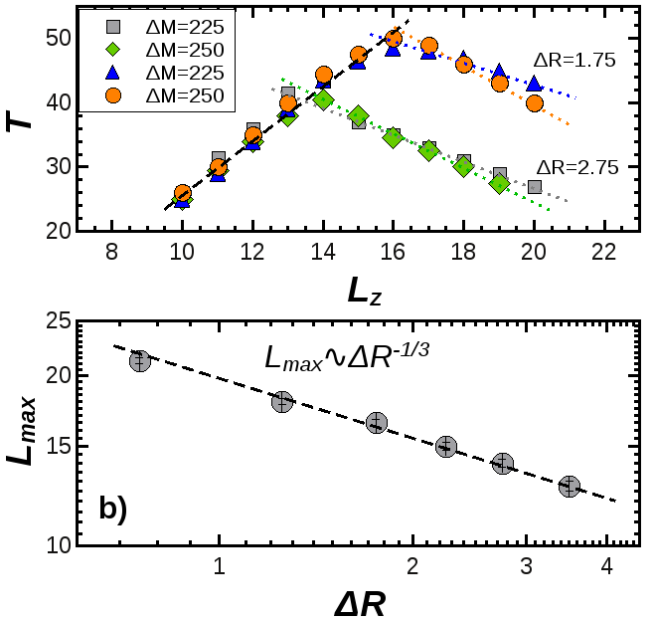

Figure 11. a) Tent-shaped profile of the oscillation period, T as a function of the reactor height L_z for two different values of ΔM and ΔR. b) Dependence of L_{max} on ΔR.

conditions, without any external feed or chemical nonlinearity, expanding thereby the possibility of chemical oscillations to ubiquitous bimolecular reactions. The trigger for the onset of this oscillatory instability is the hydrodynamic feedback promoted *in-situ* by the chemical reaction, that increases the surface tension across the reactive zone, thus promoting a Marangoni convergent flow at the liquid-air interface and, by continuity, a quasi-horizontal return flow into the reactor bulk. Chemically-driven Marangoni convection produces *damped* oscillations. The competition between the Marangoni-driven compressing force and transversely upwardly oriented RD relaxation that sustains the oscillatory mechanism is weak and the oscillations smoothen-down quickly. The presence of antagonistic buoyancy-driven flows can counter-balance Marangoni forcing and further enhance oscillations, leading to *chemo-Marangoni-buoyancy-driven sustained oscillations*.

In closed reactors, both periodic scenarios are transient. However *sustained* oscillations due the chemo-Marangoni-buoyancy interplay can be stabilized in open reactors with a constant lateral feeding of fresh reactants, while chemo-Marangoni waves intrinsically dampen-out even if the chemical reaction is kept far-from-equilibrium. The analysis presented here allows to isolate critical conditions for the oscillatory instability and provide useful information with a view to experimental realizations of chemohydrodynamic waves.

Chemo-Marangoni oscillations occur when a sufficiently large surface tension gradient ($\Delta M > \Delta M_{crit}$) is established across the localized reactive zone. With relation (24), we found that this condition may not necessarily require a dramatically different surface tension between fresh reactants and the product, provided that the surface tension of the pure reactants solution is small enough. In this case the reactive process consumes the surfactant and drives the local surface tension increase. This extends therefore the number of possible candidates for an experimental implementation of the phenomenon. The reactor height, L_z, represents a critical parameter that, by balancing the transverse competition between the reaction-diffusion processes and convective flows, can control the onset and the properties of chemo-Marangoni waves. L_z has to be larger than a minimal threshold L_c which scales as $L_c \sim \Delta M^{-1}$.

L_c turns to be a useful reference to predict the onset of chemo-Marangoni-buoyancy-driven oscillations as well. This scenario relies on a delicate balance between surface-tension-driven compression and buoyancy-driven relaxation, where the former has to be dominat-

ing. This condition is satisfied when the position of the stagnation point, Sp, locating the relative extent of Marangoni- and buoyancy-controlled domains, is such that $(L_z - Sp) > L_c$. The antagonism between the two convective forces at play can be tuned *via* ΔR (i.e. controlling the density gradient between the reacted and unreacted areas). Increasing this parameter drives a transition from *sustained* to *damped* oscillations, and eventually leads to suppress completely the oscillatory mechanism. Throughout this route towards oscillation extinction, the oscillation period drops because increasing ΔR reduces the extent of Marangoni-related convective rolls which characteristic length determines the oscillation period. The latter shows a fingerprinting tent-shaped profile over the L_z domain, with a maximum at L_{max} marking the switch from the fully Marangoni- to Marangoni-buoyancy-controlled regimes. L_z and ΔR exert a coherent impact on buoyancy intensity accounted by the relation $\Delta R^{1/3}\, L_{max} = \text{const}$.

The analysis of the oscillation period suggests that surface-tension-driven convection is the key phenomenon at the basis of chemohydrodynamic oscillations (either *damped* or *sustained* ones), mainly imposing critical conditions for their possible occurrence and their characteristic space length and oscillation period.

The dispersion relations of chemohydrodynamic waves that characterizes the wave speed v_p as a function of the wavelength show a strong dependence on the reactor height, expressed by the relative wavelength L_z/λ. This is different from typical RD chemical waves, where the wave speed only depends on the characteristic wavelength of the wave train. The functional dependence is also reversed: in the chemo-Marangoni scenario, short-wavelength waves (long relative wavelength L_z/λ) propagate faster, following the typical dispersion relation of surface-tension-driven hydrodynamic waves.

In analogy with the period dependence on L_z, in chemo-Marangoni-buoyancy waves, the dispersion relation presents two distinct branches with a drastically different scaling that allows to discriminate between different regimes. Buoyancy forces are effective when the relative wavelength $L_z/\lambda > 0.5$. Combined to the information given by the oscillation period, data taken at different reactor depths further indicates that coherent patterns of this oscillatory scenario are mainly located at the top-half of the reactor.

As a whole, the dispersion relations reveal the hydrodynamic nature of the oscillatory phenomena described in this paper. However, differently from classical cases where Marangoni stresses can promote oscillations thanks to an externally imposed constant spatial gradient of temperature[52], here the localized reaction works as an autonomous and self-propagating source of surface tension (and density) gradients that activate convective flows unstable towards oscillatory instabilities. A hierarchy of the main ingredients at play in this chemo-hydrodynamic interplay can be established: (*i*) the reactive source is the essential primer of the phenomenon, sustaining localized surface and density gradients; (*ii*) the resulting Marangoni flows undergo the oscillatory instability, thus determining the instability critical condition and the wave characteristic length; (*iii*) buoyancy-driven flows feature a feedback that sustains oscillations and modulate their properties.

Chemical oscillations in this system are therefore the result of shifting from kinetic to hydrodynamic complexity.

Experimental implementation of chemo-hydrodynamic oscillations

The mechanism discussed above presents a broad interest because the chemical scheme used can be tailored to any second-order process and its simplicity paves the way for the experimental isolation of such a class of oscillators.

Proof-of-concept experiments can be devised taking into account the minimal ingredients described above (mainly localization of the reactive source, that has to sustain a large surface-tension gradient). Labscale model systems may thus include processes that also induce thermal contributions. In general, temperature gradients can affect the local surface tension and density of a fluid in a similar way as concentration fields (solutal contribution). A local decrease of temperature normally increases the surface tension and the density. When surface tension (and density) changes are prevalently induced by thermal effects due to chemical or dissolution processes, the resulting spatio-temporal dynamics should adhere qualitatively to those predicted with our model, with temperature and flow pulsations in place of concentration waves[52]. Chemo-Marangoni-driven oscillations could be then obtained in very shallow quasi-2D reactors (or in microgravity flights) through endothermic processes (where solutal effects can be neglected) such as the endothermic alkyl-formate hydrolysis[57] or dissolution of salts like NH_4NO_3. Although a quantitative description in these systems needs to include proper thermal and energy parameters, the resulting framework is isomorphic to the isothermal model presented above.

The presence of thermal contribution introduces a further degree of freedom when it combines to solutal effects. Their global effect will be a weighted composition of these two contributions and depends on the way they combine, i.e. whether cooperatively or antagonistically. If one of these two contributions is uncoupled from the chemical source, their relative effect can be tuned and oriented at will. For example, photochemical isomerization of thermoreversible photochromic spiro-oxazine or azobenzene surfactant molecules are associated with a considerable and tunable increase of surface-tension, that can be maintained in far-from-equilibrium conditions under constant irradiation[58,59]. With this kind of systems, the heat provided by a localized irradiation to promote the photochemical transformation can also induce a density decrease, providing antagonistic buoy-

ancy forces that match minimal conditions for chemo-Marangoni-buoyancy oscillations.

VI. CONCLUSIONS

The mechanisms presented in this paper not only address the initial question whether emergent oscillatory behaviors are possible without nonlinear kinetic feedback, but they also open the perspective of a new paradigm for chemical patterns formation, including stationary structures, based on a simple chemistry. The chance for finding these patterns relies on expanding the parametric exploration of the chemohydrodynamic interplay, that so far has been restricted to the specific antagonism described by $\Delta M, \Delta R > 0$ (quadrant I of the parameter space of Fig.5). The reverse antagonism (the reaction decreases the surface tension and can increase the local density) when $\Delta M, \Delta R < 0$ and cooperative scenarios with both chemically-driven contribution to the flow oriented in the same direction ($\Delta M > 0, \Delta R < 0$ and *viceversa*) are under current analysis. Preliminary results show that even in these cases, chemohydronamics can bear emergent oscillatory behaviors, confirming the generality of this mechanism as a source of complexity. Chemohydrodynamic waves can be further generalized by considering different specific properties and combinations of the chemical species (δ_i, R_i, M_i). Check simulations in this regard show that we can complicate the dynamics with asymmetric evolution of the concentration fields, though the main ultimate dynamical features remain preserved.

Our theoretical framework can guide the interpretation of similar periodic dynamics observed in several contexts with both fundamental and applied relevance. To name a few, pulsations have been found at microscopic level in crystals undergoing dissolution in a host solution[60]. This complex kinetics in the release of matter due to the surface reactivity can impact many different processes ranging from corrosion to pharmaceutical bioavailability. Our study enlarges the comprehension and the panorama of waves triggered by surface-driven convection found in non-reactive systems[61–63]. Oscillatory dynamics indeed occur in self-propulsion of particles powered by dissolution-driven Marangoni flows[13], thus affecting the efficiency and predictability of the motion.

The identification and control of oscillatory instabilities driven by chemo-hydrodynamics is also key for the optimization of industrial processes involving heat and/or mass transfer across reactive interfaces, in which natural and Marangoni convection play an important or even a dominant role. An example is represented by crystal growth techniques[52]. It has been already shown how the efficiency of this kind of processes, pointing at growing high-quality single crystals with uniform material properties, is challenged by the formation of striations or segregation bands due to the onset of thermally-induced Marangoni and natural oscillatory convection.

From the fundamental viewpoint chemohydrodynamic mechanisms can be exploited to engineer new viable pathways to chemical oscillators with simple reactions that, as mentioned in the introduction, can be used in turn to approach transport of chemical information and signalling as well as to actuate reactive fluids and films. Finally, the simplicity of the proposed mechanisms for self-organized structures can impact and stimulate new studies in areas as fascinating as Origin of Life, where one of the main challenges resides in identifying plausible scenarios for emergent chemical structures and early functional behaviors in contexts characterized by a minimal chemistry.

SUPPLEMENTARY MATERIAL

See Supplementary Material for illustrative movies of chemo-Marangoni- and chemo-Marangoni-buoyancy-driven pulsations.

DATA AVAILABILITY STATEMENT

The data that support the findings of this study are available from the corresponding author upon reasonable request.

ACKNOWLEDGMENTS

M.A.B. gratefully acknowledges funding from Programma Operativo Nazionale (PON) Ricerca e Innovazione 20142020, Asse I Capitale Umano, Azione I.2 A.I.M. Attrazione e mobilita dei ricercatori, Linea 2 (Attrazione dei Ricercatori). Funding by Prodex, F.R.S.-FNRS, and the Fondation ULB is also gratefully acknowledged.

REFERENCES

[1] G. Nicolis and I. Prigogine, *Self-Organization in Nonequilibrium Systems* (Wiley, New York, 1977).
[2] E. Pálsson and C. E Cox, "Origin and evolution of circular waves and spirals in dictyostelium discoideum territories," Proc. Natl. Acad. Sci. **93**, 1151–1155 (1996).
[3] G. Kastberger, E. Schmelzer, and I. Kranner, "Social waves in giant honeybees repel hornets," PLoS One **3**, e3141 (2008).
[4] A. F. Taylor, M. R. Tinsley, F. Wang, Z. Huang, and K. Showalter, "Dynamical quorum sensing and synchronization in large populations of chemical oscillators," Science **323**, 614–617 (2009).
[5] V. K. Vanag, ""cognitive" modes in small networks of almost identical chemical oscillators with pulsatile inhibitory coupling," Chaos **29**, 033106 (2019).
[6] M. A. Budroni, K. Torbensen, S. Ristori, A. Abou-Hassan, and F. Rossi, "Membrane structure drives synchronization patterns in arrays of diffusively coupled self-oscillating droplets," J. Phys. Chem. Lett. **11**, 2014–2020 (2020).

[7]K. Gizynski and J. Gorecki, "Cancer classification with a network of chemical oscillators," Phys. Chem. Chem. Phys. **19**, 28808–28819 (2017).
[8]P. L. Gentili, M. S. Giubila, and B. M. Heron, "Processing binary and fuzzy logic by chaotic time series generated by a hydrodynamic photochemical oscillator," Chem. Phys. Chem. **18**, 1831–1841.
[9]J. Horváth, I. Szalai, J. Boissonade, and P. De Kepper, "Oscillatory dynamics induced in a responsive gel by a non-oscillatory chemical reaction: experimental evidence," Soft Matter **7**, 8462–8472 (2011).
[10]R. Yoshida, "Self-oscillating gels driven by the Belousov-Zhabotinsky reaction as novel smart materials," Adv. Mater. **22**, 3463–3483 (2010).
[11]A. Isakova and K. Novakovic, "Pulsatile release from a flat self-oscillating chitosan macrogel," J. Mater. Chem. B **6**, 5003–5010 (2018).
[12]S. Nakanishi, S.-i. Sakai, T. Nagai, and Y. Nakato, "Macroscopically uniform nanoperiod alloy multilayers formed by coupling of electrodeposition with current oscillations," J. Phys. Chem. B **109**, 1750–1755 (2005).
[13]T. Bánsági, M. M. Wrobel, S. K. Scott, and A. F. Taylor, "Motion and interaction of aspirin crystals at aqueous-air interfaces," J. Phys. Chem. B **117**, 13572–13577 (2013).
[14]M. A. Budroni, E. Biosa, S. Garroni, G. R. C. Mulas, N. Marchettini, N. Culeddu, and M. Rustici, "Understanding oscillatory phenomena in molecular hydrogen generation via sodium borohydride hydrolysis," Phys. Chem. Chem. Phys. **15**, 18664–18670 (2013).
[15]M. A. Budroni, S. Garroni, G. Mulas, and M. Rustici, "Bursting dynamics in molecular hydrogen generation via sodium borohydride hydrolysis," J. Phys. Chem. C **121**, 4891–4898 (2017).
[16]A. W. Hauser, S. Sundaram, and R. C. Hayward, "Photothermocapillary oscillators," Phys. Rev. Lett. **121**, 158001 (2018).
[17]P. Gray and S. K. Scott, *Chemical Oscillations and Instabilities. Non-linear Chemical Kinetics* (Oxford University Press, Oxford, UK, 1994).
[18]I. R. Epstein and K. Showalter, "Nonlinear chemical dynamics: oscillations, patterns and chaos," J. Phys. Chem. **100**, 13132–13147 (1996).
[19]R. Lefever, G. Nicolis, and P. Borckmans, "The Brusselator: it does oscillate all the same," J. Chem. Soc., Faraday Trans. 1 **84**, 1013–1023 (1988).
[20]B. P. Belousov, "A periodic reaction and its mechanism," in *Sbornik Referatov po Radiatsonno Meditsine* (Medgiz, Moscow, 1958) pp. 145–147.
[21]I. R. Epstein, K. Kustin, D. Kepper, P., and M. Orbán, "Oscillating chemical reactions," Sci. Am. **248**, 112–123 (1983).
[22]M. A. Budroni, V. Upadhyay, and L. Rongy, "Making a simple A+B→C reaction oscillate by coupling to hydrodynamic effect," Phys. Rev. Lett. **122**, 244502 (2019).
[23]A. De Wit, K. Eckert, and S. Kalliadasis, "Introduction to the focus issue: Chemo-hydrodynamic patterns and instabilities," Chaos **22**, 037101 (2012).
[24]J. A. Pojman and I. R. Epstein, "Convective effects on chemical waves. 1. mechanisms and stability criteria," J. Phys. Chem. **94**, 4966–4972 (1990).
[25]D. A. Vasquez, J. W. Wilder, and B. F. Edwards, "Convective turing patterns," Phys. Rev. Lett. **71**, 1538–1541 (1993).
[26]L. Rongy, G. Schuszter, Z. Sinkó, T. Tóth, D. Horváth, A. Tóth, and A. De Wit, "Influence of thermal effects on buoyancy-driven convection around autocatalytic chemical fronts propagating horizontally," Chaos **19**, 023110 (2009).
[27]L. Rongy and A. De Wit, "Buoyancy-driven convection around exothermic autocatalytic chemical fronts traveling horizontally in covered thin solution layers," J. Chem. Phys. **131**, 184701 (2009).
[28]L. Rongy, P. Assemat, and A. De Wit, "Marangoni-driven convection around exothermic autocatalytic chemical fronts in free-surface solution layers," Chaos **22**, 037106 (2012).
[29]M. A. Budroni, L. Rongy, and A. De Wit, "Dynamics due to combined buoyancy- and marangoni-driven convective flows around autocatalytic fronts," Phys. Chem. Chem. Phys. **14**, 14619–14629 (2012).
[30]L. Šebestíková and M. J. Hauser, "Buoyancy-driven convection may switch between reactive states in three-dimensional chemical waves," Phys. Rev. E. **85**, 036303 (2012).
[31]L. Rongy and A. De Wit, "Steady marangoni flow traveling with chemical fronts," J. Chem. Phys. **124**, 164705 (2006).
[32]L. Rongy and A. De Wit, "Solitary marangoni-driven convective structures in bistable chemical systems," Phys. Rev. E **77**, 046310 (2008).
[33]F. Rossi, M. A. Budroni, N. Marchettini, and J. Carballido-Landeira, "Segmented waves in a reaction-diffusion-convection system," Chaos **22**, 037109 (2012).
[34]M. A. Budroni, M. Masia, M. Rustici, N. Marchettini, and V. Volpert, "Bifurcations in spiral tip dynamics induced by natural convection in the Belousov-Zhabotinsky reaction," J. Chem. Phys. **130**, 024902 (2009).
[35]L. Gálfi and Z. Rácz, "Properties of the reaction front in an A+B→C type reaction-diffusion process," Phys. Rev. A **38**, 3151–3154 (1988).
[36]Z. Jiang and C. Ebner, "Simulation study of reaction fronts," Phys. Rev. A **42**, 7483–7486 (1990).
[37]B. Grzybowski, *Chemistry in Motion: Reaction-Diffusion Systems for Micro- and Nanotechnology* (Wiley, Chichester, UK, 2009).
[38]Q. Wang and O. Steinbock, "Materials synthesis and catalysis in microfluidic devices: Prebiotic chemistry in mineral membranes," ChemCatChem **12**, 63–74 (2020).
[39]C. Almarcha, P. M. J. Trevelyan, P. Grosfils, and A. De Wit, "Chemically driven hydrodynamic instabilities," Phys. Rev. Lett. **104**, 044501 (2010).
[40]L. Lemaigre, M. A. Budroni, L. A. Riolfo, P. Grosfils, and A. De Wit, "Asymmetric Rayleigh-Taylor and double-diffusive fingers in reactive systems," Phys. Fluids **25**, 014103 (2013).
[41]R. Tiani and L. Rongy, "Influence of Marangoni flows on the dynamics of isothermal A + B → C reaction fronts," J. Chem. Phys. **145**, 124701 (2016).
[42]R. Tiani, A. De Wit, and L. Rongy, "Surface tension- and buoyancy-driven flows across horizontally propagating chemical fronts," Adv. Colloid Interface Sci. **255**, 76–83 (2018).
[43]T. Gérard and A. De Wit, "Miscible viscous fingering induced by a simple $A + B \rightarrow C$ chemical reaction," Phys. Rev. E **79**, 016308 (2009).
[44]L. Rongy, P. M. J. Trevelyan, and A. De Wit, "Dynamics of A+B→C reaction fronts in the presence of buoyancy-driven convection," Phys. Rev. Lett. **101**, 084503 (2008).
[45]Y. Nagatsu, Y. Ishii, Y. Tada, and A. De Wit, "Hydrodynamic fingering instability induced by a precipitation reaction," Phys. Rev. Lett. **113**, 024502 (2014).
[46]M. A. Budroni and A. De Wit, "Localized stationary and traveling reaction-diffusion patterns in a two-layer A+B→ Oscillator system," Phys. Rev. E **93**, 062207 (2016).
[47]M. A. Budroni, L. Lemaigre, D. M. Escala, A. P. Muñuzuri, and A. De Wit, "Spatially localized chemical patterns around an A + B → Oscillator front," J. Phys. Chem. A **120**, 851–860 (2016).
[48]D. M. Escala, M. A. Budroni, J. Carballido-Landeira, A. De Wit, and A. P. Muñuzuri, "Self-organized traveling chemo-hydrodynamic fingers triggered by a chemical oscillator," J. Phys. Chem. Lett. **5**, 413–418 (2014).
[49]M. A. Budroni and A. De Wit, "Dissipative structures: From reaction-diffusion to chemo-hydrodynamic patterns," Chaos **27**, 104617 (2017).
[50]C. Rana and A. De Wit, "Reaction-driven oscillating viscous fingering," Chaos **29**, 043115 (2019).
[51]D. W. Peaceman and H. H. Rachford, "The numerical solution of parabolic and elliptic differential equations," J. Soc. Ind. Appl. Math. **3**, 28 (1955).

[52]M. K. Smith and S. H. Davis, "Instabilities of dynamic thermocapillary liquid layers. part 1. convective instabilities," J. Fluid Mech. **132**, 119–144 (1983).
[53]N. Manz, S. C. Muller, and O. Steinbock, "Anomalous dispersion of chemical waves in a homogeneously catalyzed reaction system," J. Phys. Chem. A **104**, 5895–5897 (2000).
[54]M. A. Budroni and F. Rossi, "A novel mechanism for in situ nucleation of spirals controlled by the interplay between phase fronts and reaction-diffusion waves in an oscillatory medium," J. Phys. Chem. C **119**, 9411–9417 (2015).
[55]P. Ortoleva and J. Ross, "Phase waves in oscillatory chemical reactions," J. Chem. Phys. **58**, 5673–5680 (1973).
[56]H. Lamb, *Hydrodynamics* (Dover publications, New York, 1945).
[57]M. A. Budroni, C. Thomas, and A. De Wit, "Chemical control of dissolution-driven convection in partially miscible systems: nonlinear simulations and experiments," Phys. Chem. Chem. Phys. **19**, 7936–7946 (2017).
[58]S. Santer, "Remote control of soft nano-objects by light using azobenzene containing surfactants," J. Phys. D: Appl. Phys. **51**, 013002 (2018).
[59]P. L. Gentili, M. Dolnik, and I. Epstein, "Photochemical oscillator: Colored hydrodynamic oscillations and waves in a photochromic system," J. Phys. Chem. C **118**, 598–608 (2014).
[60]C. Fischer and A. Luttge, "Pulsating dissolution of crystalline matter," Proc. Natl. Acad. Sci. **115**, 897–902 (2018).
[61]V. I. Kovalchuk, H. Kamusewitz, D. Vollhardt, and N. M. Kovalchuk, "Auto-oscillation of surface tension," Phys. Rev. E **60**, 2029–2036 (1999).
[62]K. Schwarzenberger, S. Aland, H. Domnick, S. Odenbach, and K. Eckert, "Relaxation oscillations of solutal marangoni convection at curved interfaces," Colloids Surf. A **481**, 633–643 (2015).
[63]B. Nanzai, D. Terashita, Y. Koyano, H. Kitahata, and M. Igawa, "Spontaneous electrical oscillation in horizontal three-phase liquid membrane systems: Effect of marangoni effect induced by buoyant convection," Colloids Surf. A **553**, 496 – 502 (2018).